Front. Mech. Eng. 2022, 17(1): 6
https://doi.org/10.1007/s11465-021-0662-2

RESEARCH ARTICLE

Development of lunar regolith composite and structure via laser-assisted sintering

Hua ZHAO[a], Lu MENG[b], Shaoying LI[a], Jihong ZHU (✉)[a,c], Shangqin YUAN (✉)[a,d], Weihong ZHANG[a]

[a] *State IJR Center of Aerospace Design and Additive Manufacturing, School of Mechanical Engineering, Northwestern Polytechnical University, Xi'an 710072, China*
[b] *Beijing Institute of Radio Measurement, Beijing 100854, China*
[c] *Key Laboratory of Metal High Performance Additive Manufacturing and Innovative Design, MIIT China, Northwestern Polytechnical University, Xi'an 710072, China*
[d] *Unmanned System Research Institute, Northwestern Polytechnical University, Xi'an 710072, China*

✉ *Corresponding author. E-mails: jh.zhu@nwpu.edu.cn (Jihong ZHU); shangqin.yuan@nwpu.edu.cn (Shangqin YUAN)*

ABSTRACT Aiming at the exploration and resource utilization activities on the Moon, *in situ* resource utilization and *in situ* manufacturing are proposed to minimize the dependence on the ground transportation supplies. In this paper, a laser-assisted additive manufacturing process is developed to fabricate lunar regolith composites with PA12/SiO_2 mixing powders. The process parameters and composite material compositions are optimized in an appropriate range through orthogonal experiments to establish the relationship of process–structure–property for lunar regolith composites. The optimal combination of composite material compositions and process parameters are mixing ratio of 50/50 in volume, laser power of 30 W, scanning speed of 3500 mm/s, and scanning hatch space of 0.2 mm. The maximum tensile strength of lunar regolith composites reaches 9.248 MPa, and the maximum depth of surface variation is 120.79 μm, which indicates poor powder fusion and sintering quality. Thereafter, the mechanical properties of laser-sintered lunar regolith composites are implemented to the topology optimization design of complex structures. The effectiveness and the feasibility of this laser-assisted process are potentially developed for future lightweight design and manufacturing of the solar panel installed on the lunar rover.

KEYWORDS *in situ* manufacturing, laser-assisted powder fusion process, mechanical properties, topological structure design

1 Introduction

Deep-space exploration [1] usually includes the exploration and the resource utilization activities of the Moon and other celestial bodies in space. The major spacefaring nations have formulated deep-space exploration missions for 20 years and beyond [2,3]. The Moon, as Earth's only natural satellite, is the first target for human extraterrestrial celestial body detection and resource utilization, and has turned into a springboard and a refueling stopover for humans to explore outer space. However, the expenditure to transport probes and raw materials from the ground to the Moon surface is immense due to the long distance. Thus, minimizing the ground transportation supplies and the energy consumption is necessary. Therefore, lunar *in situ* resource utilization and *in situ* manufacturing are proposed to use *in situ* resources fully and fabricate structural/functional components for future civilization [4–7]. *In situ* exploitation of lunar resources is helpful for developing the space resident structures and promoting the fabrication, repair [8,9], and replacement of aerospace parts [10], thus reducing the spare parts brought from Earth and lightening the material quality and volume. In addition, this approach can create considerable economic savings and reduce the risk of exploration missions [11].

Lunar concrete, mainly composed of lunar regolith and rocks, can be developed as an architectural material due to its unique advantages such as thermal and radiation shielding [12–15]. Research works have been conducted on the feasibility of conventional and additive manufacturing (AM) processes utilizing lunar concrete as raw materials for construction and functional structures'

Received May 15, 2021; accepted October 22, 2021

production in the future lunar base [16–18], including microwave technology [19,20], laser sintering [21,22], and compression molding [23]. Simultaneously, several studies characterized the microstructure of lunar regolith composite materials and measured their thermal performance, durability performance, and mechanical properties [24–26]. Liu et al. [27] analyzed the microstructure, chemical composition, particle size distribution, and thermogravimetric characteristics of CLRS-2 lunar weathering layer simulant, and improved its compressive capacity and fracture strength.

Additionally, the D-shape process was investigated by Cesaretti et al. [28] to establish a human-inhabitable base on the Moon. A special "ink" was employed in the D-shape process to overcome the cohesive inertness of sand-based condensed material to make them agglomerate. However, forming parts in the extreme environment of microgravity in space still has great challenges and uncertainties. Meurisse et al. [29] implemented solar AM technology to fabricate bricks layer by layer using imitation moondust materials under the high temperature of 1000 °C in a solar furnace. Unexpectedly, the printed brick structure showed a warping effect and a poor accuracy due to the integral forming in the uneven temperature field. In a recent work, Liu et al. [27] mixed CLRS-2 lunar weathering layer simulant powders and light-curing resin to make architectural and functional structures by using digital light processing (DLP) technology. However, volume shrinkage and poor forming accuracy were observed after sintering, and a relatively large quantity of resin material was required owing to the evaporation during sintering, which adversely influenced the exploitation of *in situ* resources and is not recommended for *in situ* manufacturing.

To realize the *in situ* AM of lunar regolith on the Moon, the influence of the lunar low-gravity environment on the AM process has to be considered. At present, relevant studies have verified the feasibility of AM processes under different gravity environments through parabolic tests of airplanes or in space stations [30,31]. In 2018, the researchers from the Chinese Academy of Sciences achieved the world's first 3D printing experiment of ceramic materials under microgravity conditions by utilizing DLP technology, which proved the feasibility of this process [27]. The 3D printer developed by the Fifth Academy of Aerospace Science and Technology Group, China independently completed the first sample printing of continuous fiber-reinforced composite materials worldwide and verified the scientific experiment goal of 3D printing of composite materials in a microgravity environment. Reitz et al. [32] conducted selective laser melting experiments of regolith simulation under different gravitational conditions with the Einstein-Elevator equipment, which did not show any major differences in the geometry, mass, and porosity of the samples.

Thereafter, to utilize the advantages of *in situ* resource utilization and *in situ* manufacturing for deep-space exploration fully, a laser-assisted AM process is proposed to fabricate 3D solid structural components with complex geometries using the mixed powders of lunar regolith and the polymer binder. Compared with the previous approach, the laser-assisted process shows its unique advantages for *in situ* manufacturing as follows [33]. First, it possesses high forming accuracy and a uniform temperature field, which avoids forming defects such as large deformation and warping of the structure. Second, it exhibits high efficiency of material and energy utilization, rapid speed of manufacturing, and a wide range of available materials. Finally, on the Moon, lunar regolith composite powders are spread on the powder bed for *in situ* manufacturing, which is conveniently generated by the vacuum environment and adaptable to the influence of low gravity.

In this work, a new process is proposed to fabricate lunar regolith composites through laser-assisted technology [34–37] and utilize them for deep-space exploration, which is the key to achieving basic component production and base construction on the Moon. The laser-assisted fusion with the advantages of diversified materials, low cost, fast production speed, and high forming accuracy can maximize the utilization of lunar regolith, and reduce the demand for energy consumption. The size distribution and surface morphology of the composite powders are characterized by a scanning electron microscope (SEM), confirming a relatively approximate size distribution of the PA12 and SiO_2 powders. The thermal properties including the temperatures of melting, recrystallization, and decomposition are characterized by differential scanning calorimetry (DSC) and thermogravimetric analysis (TGA) to determine the temperature window of the laser-assisted process. The mechanical properties of tensile strength, elastic modulus, and Poisson's ratio of the PA12/SiO_2 mixing powders measured by orthogonal experiments are implemented on the structural design by means of topology optimization. Finally, the feasibility of laser-assisted manufacturing of lunar regolith composites is evaluated by topological lightweight design and *in situ* fabrication.

2 Materials and methods

2.1 Material preparation

SiO_2 is the main chemical constituent of lunar regolith [38] and its simulants [5,39–41] according to the analysis of lunar regolith samples excavated from different regions of the Moon by the Apollo Program. Hence, quartz sand was employed as the lunar regolith simulant in this work. Commercially available thermoplastic PA12 powders (FS3300PA, Farsoon Technologies, China) are a typical type of thermoplastic polymer used in the laser-

assisted powder fusion system. The melting point and the bulk density of PA12 are 183 °C and 1.06 g/cm^3, respectively. Quartz sand (hereinafter referred to as SiO_2) powders (purchased from Lanrun Environmental Protection Technology, China) with a diameter equal to that of PA12 were selected to blend evenly to ensure fluidity and avoid agglomeration. The composite powders were synthesized by mixing PA12 powders as the binder and SiO_2 powders with volume ratio of 50/50 in the stirrer, followed by screening with a 120-mesh gauze to remove impurities. Subsequently, the composite powders were dried in a vacuum oven at 120 °C for 2 h. Another composite powder with PA12/SiO_2 of 30/70 in volume ratio was prepared to verify the effect of the mixing ratio on the microstructure and mechanical performance of the printed sample.

2.2 Lunar regolith composite fabrication

The 3D printing was conducted on the composite powders adopting a laser-assisted machine (EP-P3850, E-Plus-3D, China), installed with a CO_2 laser (laser power p up to 50 W). Layer-by-layer deposition of the composite powders on the X–Y plane was sintered by laser heat according to the layered cross-section information under computer control, and then the structure built along Z-axis via a bottom–up process was completed by removing the unsintered powders. To investigate the process–structure–property relationship further, this work systematically studied the influence of the process parameters on the performance of the printed specimens through orthogonal experiments with four factors and three levels. The different process parameters are reported in Table 1 to study the influence of mixing ratio (r) in volume, laser power (p), scanning speed (v), and hatching space (h) on the mechanical properties of the tensile specimens in compliance with ASTM D638, Type V.

2.3 Material characterizations

A DSC experiment was carried out using DSC Instruments (DSC 200 F3, NETZSCH, Germany) under a nitrogen atmosphere as protective gas with a flow rate of 50 mL/min to measure the melting and crystallization temperature of neat PA12 and two PA12/SiO_2 composite powders. A powder sample of 5 mg was encapsulated in a standard aluminum pan and loaded into DSC for heating–cooling loop testing. The thermal program for this experiment was as follows: Cool rapidly to T = 25 °C, hold isothermally for 1 min, heat up with a rate of 10 °C/min to 250 °C, hold isothermally for 1 min, cool to T = 25 °C with a rate of 10 °C/min, hold isothermally, and finally stop. This heating–cooling procedure was conducted to identify the onset and the offset of melting and recrystallization temperature as well as the enthalpy changes during phase transitions.

Table 1 Different process parameters (mixing ratio r [PA12/SiO_2], laser power p, scanning speed v, and hatch space h) investigated in the orthogonal experiments

Level of parameter	r/%	p/W	v/(mm·s^{-1})	h/mm
1	30/70	20	3000	0.20
2	50/50	25	3500	0.25
3	100/0	30	4000	0.30

A TGA experiment was conducted using synchronous thermal analyzer (STA) equipment (STA 449 F3, NETZSCH, Germany). For each experiment, the TGA results were obtained from approximately 5 mg of neat PA12 or PA12/SiO_2 composite powders, which was sequentially heated from room temperature to 650 °C at a rate of 20 °C/min under a nitrogen gas environment to obtain the decomposition curves at high temperatures.

The SEM considered as a means of observation was provided a resolution higher than that of the optical but lower than that of transmission electron microscopy. A TM 4000 PLUS scanning electron microscopy was utilized in the high-vacuum circumstance and at a voltage of 5 kV to acquire the SEM images that characterized the morphological features of neat PA12 powders and two PA12/SiO_2 composite powders. Additionally, to inspect the quality of PA12/SiO_2 samples manufactured under the specific optimal combination of process parameters in microscale, the microstructures of standard parts that were polished by GMP-3000P grinding and polishing machine were characterized by a VHX-6000 digital optical microscope. The PA12/SiO_2 samples via synchronous thermal analyzer (SLS) for optical characterization were required to be preliminarily grounded and polished to achieve smooth, reflective surfaces.

To investigate the influence of the process parameters on the mechanical properties, nine sets of tensile specimens were manufactured under corresponding conditions to conduct uniaxial tensile experiments using TestResources^{TM} with a 100 kN load cell at the loading rate of 1 mm/min and PMLAB DIC-3D system. It is used to produce the force–displacement curves and the whole-field displacement and strain for further calculating the mechanical properties of tensile strength, elastic modulus, and Poisson's ratio. For each set of process parameters, five tensile samples were produced.

3 Results and discussion

3.1 Structural and thermal evaluation

The morphology and distribution characteristics of neat PA12 and two volume ratios of PA12/SiO_2 mixed powders are presented in Fig. 1. The neat PA12 powders with the particle size ranging from 50 to 90 μm exhibit an ellipsoidal shape and a relatively homogeneous

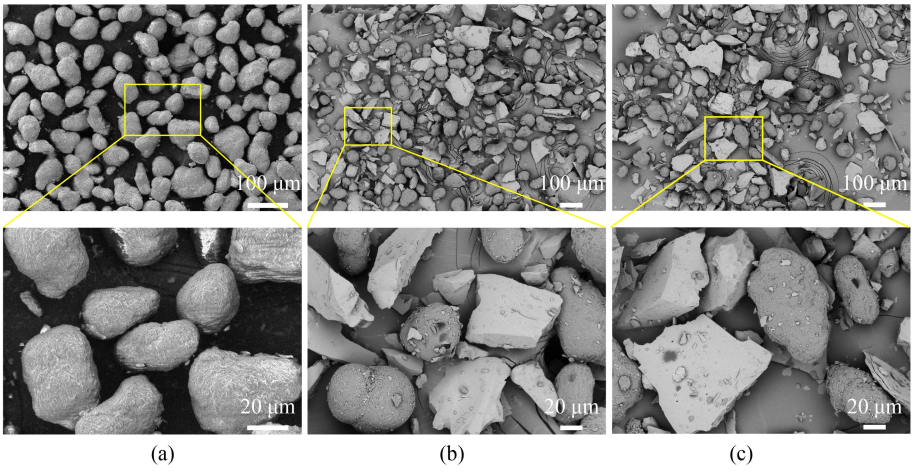

Fig. 1 SEM images of (a) neat PA12, (b) PA12/SiO_2 (50/50) composite powders, and (c) PA12/SiO_2 (30/70) composite powders.

distribution. On the contrary, the SiO_2 powders regarded as the lunar regolith simulant show an irregular shape and an uneven size distribution. However, the PA12 and SiO_2 powders possess relatively approximate size distribution and mixed evenly to guarantee the flowability of PA12/SiO_2 powders, which is remarkable for the deposition behavior of powders in the SLS process. The changes in composition can be distinctly observed in the two sets of PA12/SiO_2 powders. The mutual bonding between PA12 and SiO_2 powders is enhanced as the portion of PA12 powders increases.

DSC measurements characterize the phase transformation of melting and recrystallization of neat PA12 powders and PA12/SiO_2 powders through the endothermic and exothermic process, which provide important guidance for the temperature control of laser sintering, as illustrated in Fig. 2. The neat PA12 powders on account of their high crystallinity exhibit a very sharp melting peak and a crystallization peak accompanied with a high enthalpy of fusion and enthalpy of crystallization, respectively. By contrast, PA12/SiO_2 powders display relatively low melting and crystallization peaks, indicating that the addition of lunar regolith simulant can promote the process of melting and crystallization, reduce energy consumption and release capacity of phase change, and improve the thermal conductivity and melting efficiency of mixed powders. The PA12/SiO_2 powders show a relatively narrow recrystallization peak, which demonstrates that the lunar regolith simulant as a nucleating agent can accelerate the crystallization. The endothermic processes of the three powders show sharp endothermic peaks at 186.8, 185.9, and 185.3 °C. This finding demonstrates that the melting point temperature of the PA12/SiO_2 powders can be considered consistent with that of the neat PA12 powders. However, the recrystallization temperature rises slightly because of the reduced energy consumption of the recrystallization and crystal phase, which is also advantageous for shape retention.

The TGA and differential thermogravimetry (DTG) curves of the neat PA12 and PA12/SiO_2 mixed powders are illustrated in Fig. 3, which describes the thermal decomposition process and characterizes the loss of mass. With the continuous increment of SiO_2 powders, the following can be concluded: The onset temperature of decomposition shifts to the left from 416 to 408 °C, the temperatures of mass loss are distributed around 436 °C, and the mass loss exhibits a substantial decline from 73.5% to 17.5%. From the perspective of mass loss, a portion of the carbon remains after the decomposition of the PA12 phase, whereas the SiO_2 powders in the mixed powders are not decomposed due to their high melting point, which is quite stable within several hundred degrees Celsius. SiO_2 is the representative and the main component of lunar regolith; therefore, it also illustrates the rationality and the effectiveness of regarding SiO_2 as the lunar regolith simulant.

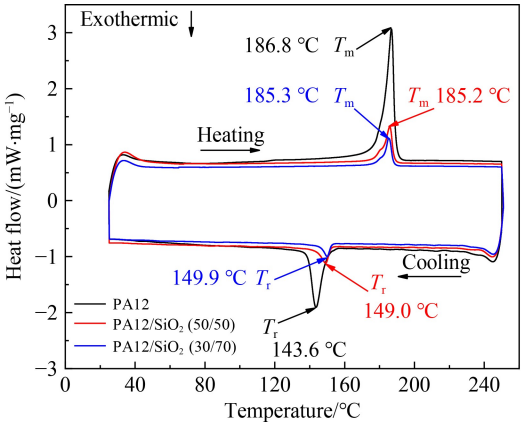

Fig. 2 DSC curves of neat PA12 and PA12/SiO_2 composite powders during the heating–cooling procedure.

The thermal properties with respect to the onset, peak, and offset of melting temperatures, crystallization temperatures, decomposition temperatures as well as the values of glass windows of the neat PA12 and PA12/SiO_2 mixed powders are calculated in Tables 2 and 3. Generally, the

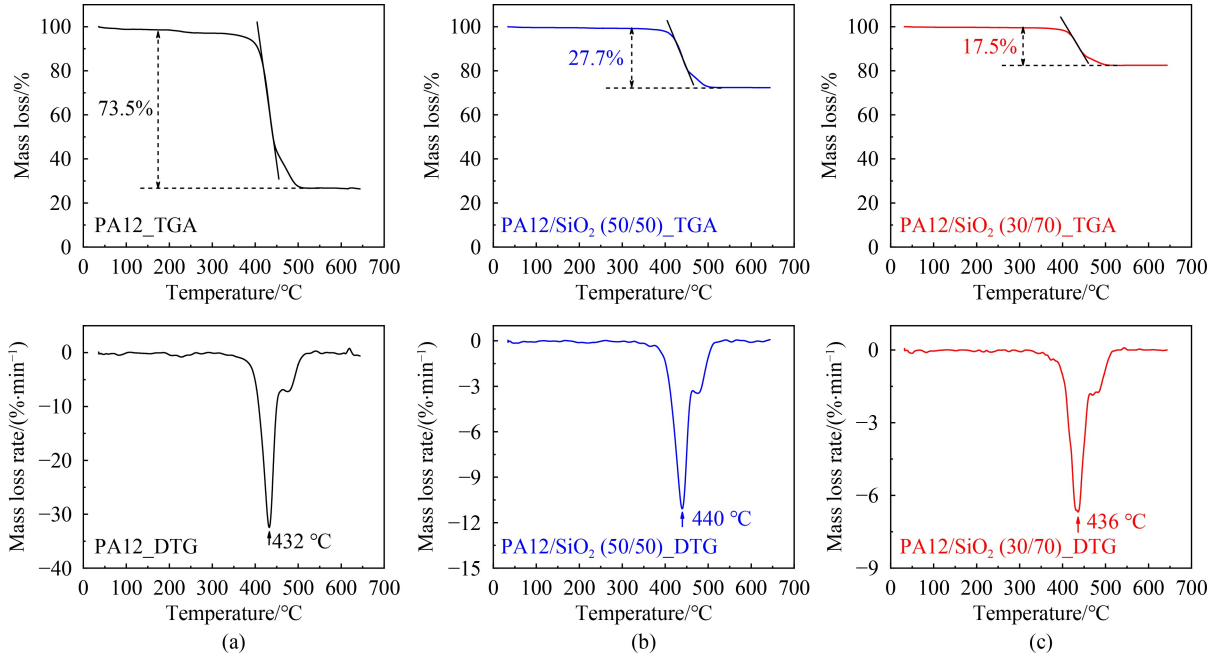

Fig. 3 TGA and DTG curves of (a) neat PA12, (b) PA12/SiO_2 (50/50) composite powders, and (c) PA12/SiO_2 (30/70) composite powders.

Table 2 Melting and recrystallization parameters of PA12 and PA12/SiO_2 composite powders

Material	Onset melting temperature/°C	Offset melting temperature/°C	Melting peak/°C	Enthalpy of melting/ ($J \cdot g^{-1}$)	Onset recrystallization temperature/°C	Offset recrystallization temperature/°C	Recrystallization peak/°C	Enthalpy of recrystallization/ ($J \cdot g^{-1}$)	Glass window width/°C
Neat PA12	181.0	189.2	186.8	101.8	139.4	149.7	143.6	33.3	31.3
PA12/SiO_2 (50/50)	181.0	188.3	185.9	28.5	144.1	152.0	149.0	5.5	29.0
PA12/SiO_2 (30/70)	181.9	188.0	185.3	18.3	146.4	152.6	150.0	5.2	29.3

Table 3 Decomposition parameters of PA12 and PA12/SiO_2 composite powders

Material	Onset decomposition temperature/°C	Offset decomposition temperature/°C	Decomposition peak/°C	Mass loss/%
Neat PA12	416	457	432	73.5
PA12/SiO_2 (50/50)	411	467	440	27.7
PA12/SiO_2 (30/70)	408	463	436	17.5

preheating temperature and the chamber temperature of the SLS process are determined before printing according to the DSC endothermic–exothermic procedure. In this work, the controlling curves of temperature for the three powders are kept the same. The temperature of the preheating and the chamber are set to 173 °C below the onset of melting temperature and 120 °C below the onset of crystallization temperature, respectively. Moreover, the glass window is defined as the temperature interval between the onsets of melting and crystallization temperatures, and the glass window of the PA12/SiO_2 mixed powders is narrower than that of the neat PA12 powders.

3.2 Mechanical properties

The engineering stress–strain curves of the tensile specimens built based on different process parameters according to the material group are shown in Fig. 4. The corresponding tensile strength, tensile modulus, and Poisson's ratio calculated by static tensile tests and digital image correlation (DIC) tests are displayed in Tables 4 and 5. Taking the tensile strength as the test index, the sum of the test index values for each factor corresponding to the three levels is calculated. The range R reflects the influence degree of corresponding factors. Overall, tensile strength declines extremely with the decreasing content of the PA12 powders. Therefore, mixing ratio, with a range of 83.595, is the most influential among the studied factors, whereas the three other factors with the range around 30 have a relatively approximate influence on tensile strength. In addition, the specimens printed with neat PA12 exhibit brittle fracture, and ductility is improved with the addition of lunar regolith simulant.

The previous investigation of *in situ* manufacturing

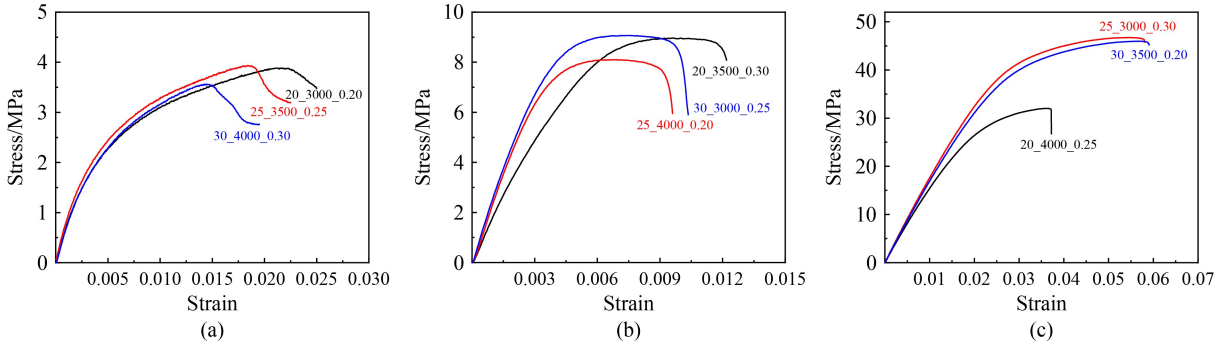

Fig. 4 Engineering stress–strain curves illustrate the influence of process parameters on tensile strength: (a) PA12/SiO_2 (30/70), (b) PA12/SiO_2 (50/50), and (c) neat PA12.

Table 4 Orthogonal experimental results on the mechanical properties of tensile specimens

No.	Mixing ratio	Laser power	Scanning speed	Hatch space	Tensile strength/MPa	Tensile modulus/MPa	Poisson's ratio
1	1	1	1	1	4.024	1676.4	0.23
2	1	2	2	2	4.120	1229.0	0.22
3	1	3	3	3	3.404	673.9	0.23
4	2	1	2	3	8.888	1533.0	0.16
5	2	2	3	1	8.680	2005.5	0.21
6	2	3	1	2	9.248	2270.2	0.20
7	3	1	3	2	16.550	862.8	0.40
8	3	2	1	3	32.018	1509.0	0.40
9	3	3	2	1	46.575	1913.8	0.43

Table 5 Analysis and calculation of the orthogonal experimental results

Level	Mixing ratio	Laser power	Scanning speed	Hatch space
I [a]	11.548	29.462	45.290	59.279
II	26.816	44.818	59.583	29.918
III	95.143	59.227	28.634	44.310
Range (R) [b]	83.595	29.765	30.949	29.361

Notes: [a] "I" represents the sum of the test index values (i.e., the tensile strength in Table 4) corresponding to the number "1" in the column where the factor is located. The same applies to II and III. [b] The range R represents the difference between the maximum and minimum values of Levels I, II, and III in each factor.

only verified the possibility of fabrication of lunar regolith composites, whereas in this paper, the process parameters were also optimized within an operation window to determine the influence of different parameters on tensile strength. In the high-temperature fabrication of lunar bricks by solar furnace carried out by the European Space Agency scientists [29], the manufactured bricks showed a warping effect and a poor accuracy; consequently, the process could not be used to make structural components. The Chinese Academy of Sciences [27] proposed employing photosensitive resin as the binder to form lunar regolith parts by using DLP technology, which caused a waste of resin materials. In comparison, the laser-assisted fusion introduced the mixing ratio in volume with the lunar regolith and PA12 powders, which could considerably reduce the mass fraction and increase the utilization rate of polymer binder, indicating the superiority of *in situ* manufacturing. Regarding the characterization of the mechanical properties of lunar regolith composites, compressive strength [42,43] and flexure strength [27] were commonly investigated in published literature. Therefore, this work discusses the characterization of tensile strength of lunar regolith samples under different sets of process parameters, which is of great importance to structural designs in lunar exploration. Tensile modulus and Poisson's ratio are innovatively measured to combine manufacturing process, mechanical performance, and structural design.

The trend chart of tensile strength varied with the factor levels can also be acquired by the orthogonal experiment. For each factor, the level numbers are taken as the abscissa, and the sum of the indicators corresponding to each level acts as the ordinate. Then, the trend charts of multiple process factors are illustrated in Fig. 5, in which the process parameter is optimized in a certain range for a single factor. The objective of this work is to utilize the lunar regolith material as much as possible while meeting the requirements of the mechanical properties to reflect the advantages of *in situ* resource utilization and provide an option for future *in situ* lunar manufacturing. The optimal process parameters are as follows: mixing ratio of 50/50 in volume, laser power of 30 W, scanning speed of 3500 mm/s, and hatch space of 0.2 mm. Thereafter, the

set of process parameters is successfully applied to the fabrication of 3D complex products. After grinding and polishing the standard part fabricated by the optimal parameters, many holes are discovered in the part with the maximum depth of 120.79 μm, as illustrated in Fig. 6. This finding indicates the poor powder fusion quality of PA12/SiO_2 composite powders and explains the reason for the notable decline in tensile strength compared with neat PA12.

To simulate the lunar environment and evaluate the feasibility of forming a lunar regolith composite using polymer binders, no surface treatment or polymeric modification is applied on the SiO_2 powders. The normal infra laser source is employed as a thermal energy generator, and no liquid and pre/post process are required in the proposed development of lunar regolith composite. The temperature facing the sunny side is higher; thus, solar energy can be directly used as the heat source of the sintering by the prism system. Compared with directly sintering lunar regolith with extremely high melting temperature over 1200 °C, the introduction of the thermoplastic polymer phase is a good strategy to glue lunar regolith and form solid, lightweight composites with minimized energy consumption. Moreover, although the mechanical properties of the printed lunar regolith composite are not compared with the neat polymer or laser sintered composites that are usually applied sophisticated pre/post treatment on feedstock powders, it is highly achievable under the extreme environmental conditions on the moon and shows a large potential in constructing the functional components with complex structures. Load-bearing structures, protective structures, and heat-insulating structures are important components of equipment and parts in lunar exploration. Therefore, these structures fabricated with the lunar regolith composite by laser-assisted fusion can well adapt to the

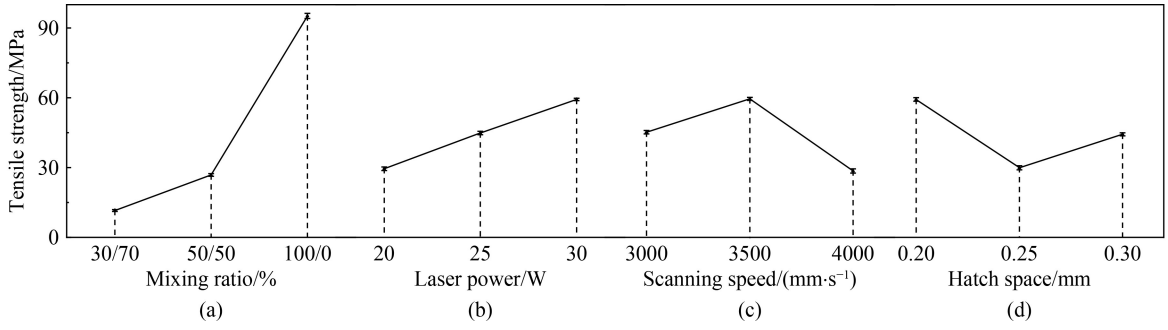

Fig. 5 Trend charts of tensile strength varied with the levels of the factors: (a) mixing ratio, (b) laser power, (c) scanning speed, and (d) hatch space.

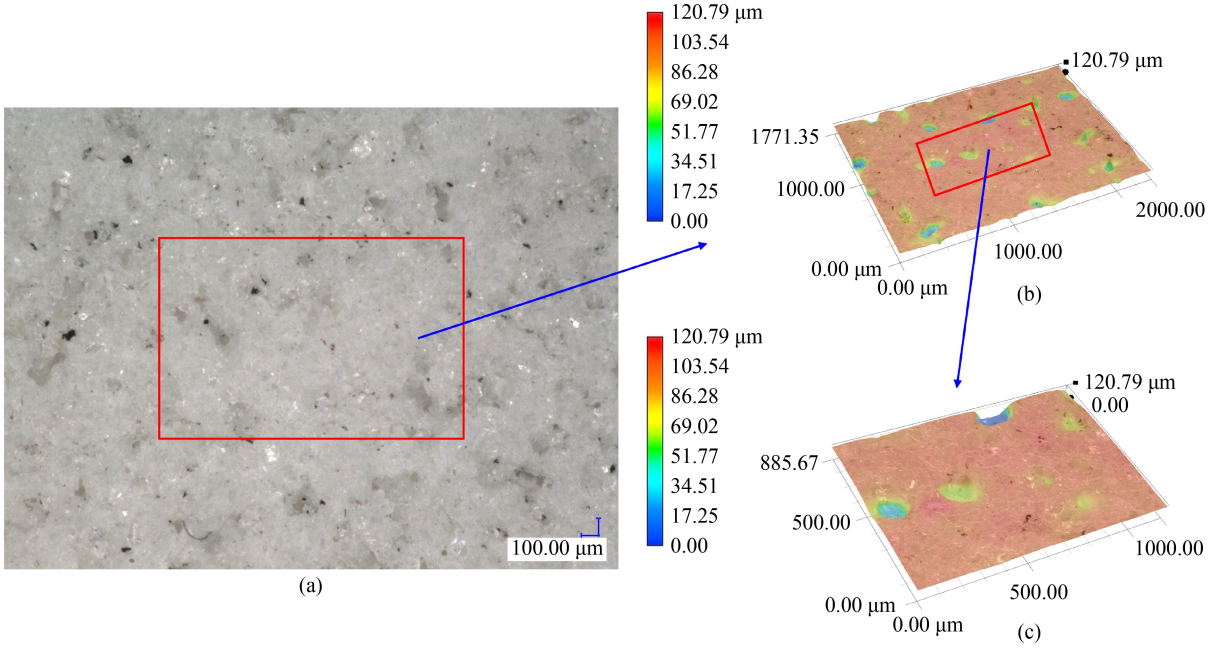

Fig. 6 (a) 2D surface of PA12/SiO_2 specimen built by optimal parameters observed under a digital optical microscope, (b) porosity characterization by 3D depth synthesis and then zoomed in to illustrate in (c).

extreme lunar environment and reduce the considerable economic costs and the risk of exploring activities.

The lightweight design of the functional and architectural structures can maximize the reduction of the weight of structures and improve the utilization of materials while meeting the requirements of performances. First, the optimal tensile modulus of 2270 MPa and Poisson's ratio of 0.20 are successfully implemented in topology optimization designs. Then, the topologically optimized structure is reconstructed by CAD software, and the mechanical properties of the reconstructed structure are simulated by the finite element method. Finally, the laser-assisted powder fusion of PA12/SiO_2 mixing powders provides a remarkable technical simulation to realize the possibility of *in situ* manufacturing of the reconstructed structures. The lightweight design and fabrication flow diagram of the solar panel installed on the lunar rover are demonstrated in Fig. 7. The finite element simulation results of the reconstructed structure show that the maximum tensile stress is 4.7 MPa, which is lower than the tensile strength of the lunar regolith composite material. This case verifies the feasibility of the proposed laser-assisted fusion in fabricating large-scale parts, satisfying the demands of the manufacturing of lightweight components with arbitrarily complex shapes and broad freedom in design.

The method of structural optimization design [44] has universal applicability while the designed structures with quite complex geometry cannot be manufactured by the traditional machining process. Then, the development of AM technology enables realizing the design and manufacture of structures. The raw material of the lunar regolith has the enormous *in situ* advantages of abundant resources and excellent suitability of extreme lunar environment, which includes wide large temperature change, vacuum, and microgravity. In addition, PA12 powders can be replaced by other polymer binders to improve structural loading performance due to the wide choice of materials of the laser-assisted fusion. Thence, the method of combining laser-assisted fusion with structural optimization design possesses broad applicability in the *in situ* resource utilization and *in situ* manufacturing on the Moon. Finally, robot technology can be integrated into the design and manufacturing method to achieve a high automation and expand its scope of application, which can provide substantial technical support for an interstellar exploration program.

4 Conclusions

In this work, a laser-assisted powder fusion for *in situ*

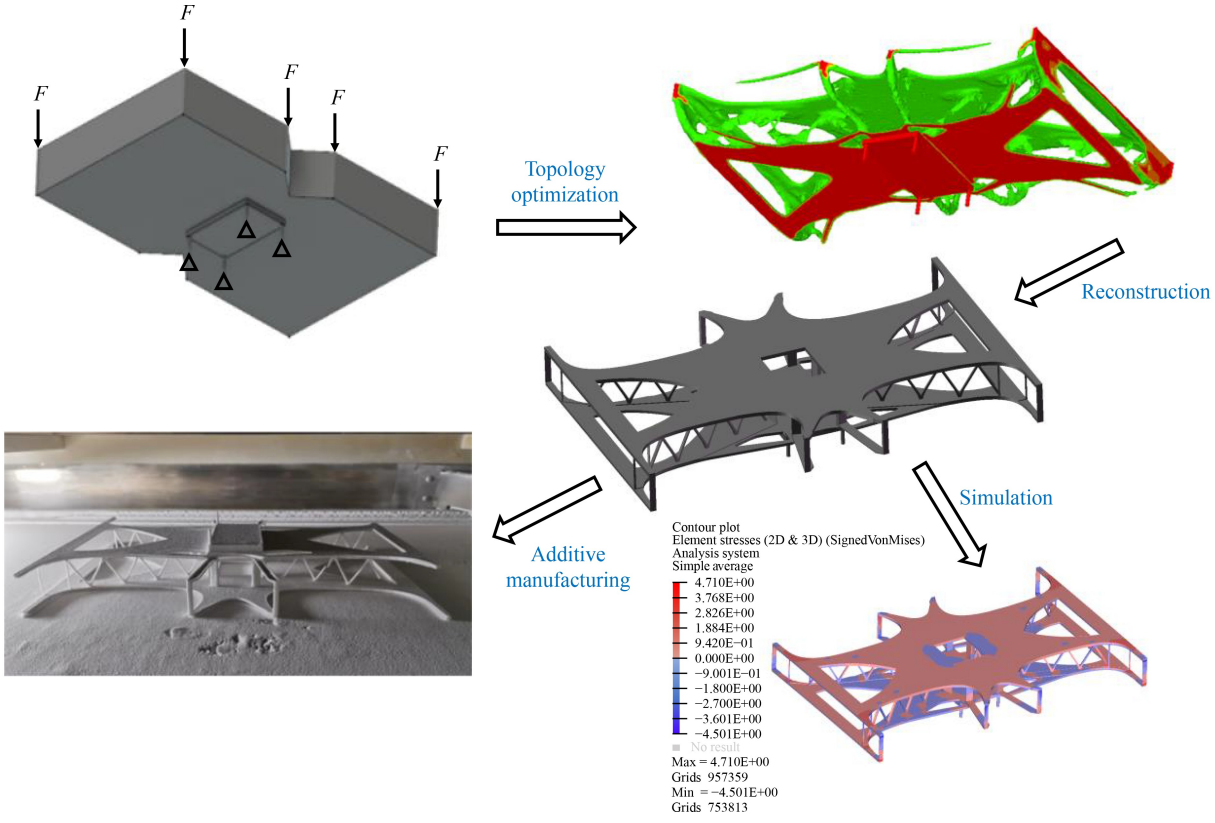

Fig. 7 Topology optimization design and manufacturing with PA12/SiO_2 composite powders of the solar panel installed on the lunar rover.

manufacturing of lunar regolith composites was successfully developed for lunar resource exploration. The process–structure–property relationship of laser-sintered lunar regolith composites was investigated to improve the tensile strength of lunar regolith composites. The mechanical properties were evaluated through systematic orthogonal experiments, by which the process parameters were optimized within an operation window of the lunar regolith composite materials. The maximum tensile strength reached 9 MPa, and a poor interfacial affinity between polymer and lunar regolith was still observed. Then, the optimized parameters of mechanical properties were successfully implemented to the structural design of the topologized structural parts and lunar base buildings. Finally, the laser-assisted powder fusion method for PA12/SiO_2 composites with the high efficiency of material utilization provided a fundamental understanding to realize the *in situ* material utilization and manufacturing on the Moon.

Acknowledgements This work was supported by the National Key R&D Program of China (Grant No. 2017YFB1102800), the National Natural Science Foundation of China for Excellent Young Scholars (Grant No. 11722219), the National Natural Science Foundation of China (Grant No. 51905439), and the Emerging (Interdisciplinary) Cultivation Project of Northwestern Polytechnical University, China (Grant Nos. 19SH030403 and 20SH030201).

Nomenclature

Abbreviations

AM	Additive manufacturing
CAD	Computer-aided design
DIC	Digital image correlation
DLP	Digital light processing
DSC	Differential scanning calorimetry
DTG	Differential thermogravimetry
ESA	European Space Agency
SEM	Scanning electron microscope
SLS	Selective laser sintering
STA	Synchronous thermal analyzer
TGA	Thermogravimetric analysis

Variables

F	External force loading on the structure
h	Hatch space
p	Laser power
r	Mixing ratio
R	Influence degree of corresponding factors
T_m	Melting peak temperature
T_r	Recrystallization peak temperature
v	Scanning speed

References

1. Wu W R, Liu W W, Qiao D, Jie D G. Investigation on the development of deep space exploration. Science China Technological Sciences, 2012, 55(4): 1086–1091
2. Xu L, Zou Y L, Jia Y Z. China's planning for deep space exploration and lunar exploration before 2030. Chinese Journal of Space Science, 2018, 38(5): 591–592
3. Howell J T, Fikes J C, McLemore C A, Good J E. On-site fabrication infrastructure to enable efficient exploration and utilization of space. In: Proceedings of International Astronautical Federation—the 59th International Astronautical Congress. Glasgow, 2008, 20090016302
4. Lee T S, Lee J, Ann K Y. Manufacture of polymeric concrete on the Moon. Acta Astronautica, 2015, 114: 60–64
5. Goulas A, Binner J G P, Harris R A, Friel R J. Assessing extraterrestrial regolith material simulants for *in-situ* resource utilisation based 3D printing. Applied Materials Today, 2017, 6: 54–61
6. Sanders G B, Larson W E. Integration of *in-situ* resource utilization into lunar/Mars exploration through field analogs. Advances in Space Research, 2011, 47(1): 20–29
7. Hintze P E, Quintana S. Building a lunar or Martian launch pad with *in situ* materials: recent laboratory and field studies. Journal of Aerospace Engineering, 2013, 26(1): 134–142
8. Bassler J A, Bodiford M P, Hammond M S, King R, Mclemore C A, Hall N R, Fiske M R, Ray J A. *In situ* fabrication and repair (ISFR) technologies; new challenges for exploration. In: Proceedings of the 44th AIAA Aerospace Sciences Meeting and Exhibit. Reno, 2006, AIAA 2006–350
9. Jessen S, Choi E, Xue L J. Development of a space manufacturing facility for *in-situ* fabrication of large space structures. In: Proceedings of the 57th International Astronautical Congress. Valencia, 2006, 1–11
10. Sanders G B, Larson W E. Progress made in lunar *in situ* resource utilization under NASA's exploration technology and development program. Journal of Aerospace Engineering, 2013, 26(1): 5–17
11. Rasera J N, Cilliers J J, Lamamy J A, Hadler K. The beneficiation of lunar regolith for space resource utilisation: a review. Planetary and Space Science, 2020, 186: 104879
12. Montes C, Broussard K, Gongre M, Simicevic N, Mejia J, Tham J, Allouche E, Davis G. Evaluation of lunar regolith geopolymer binder as a radioactive shielding material for space exploration applications. Advances in Space Research, 2015, 56(6): 1212–1221
13. Werkheiser N J, Edmunson J E, Fiske M R, Khoshnevis B. On the development of additive construction technologies for application to development of lunar/martian surface structures using *in-situ* materials. In: Proceedings of AIAA SPACE 2015 Conference and Exposition. Pasadena, 2015, AIAA 2015–4451
14. McLemore C A, Fikes J C, McCarley K S, Good J E, Kennedy J P, Gilley S D. From lunar regolith to fabricated parts: technology developments and the utilization of Moon dirt. In: Proceedings of

the 11th Biennial ASCE Aerospace Division International Conference on Engineering, Science, Construction, and Operations in Challenging Environments. Long Beach: ASCE, 2008
15. Naser M Z, Chehab A I. Materials and design concepts for space-resilient structures. Progress in Aerospace Sciences, 2018, 98: 74–90
16. Hammond M S, Good J E, Gilley S D, Howard R W. Developing fabrication technologies to provide on demand manufacturing for exploration of the Moon and Mars. In: Proceedings of the 44th AIAA Aerospace Sciences Meeting and Exhibit. Reno: AIAA, 2006, 526
17. Toutanji H, Fiske M R, Bodiford M P. Development and application of lunar "concrete"' for habitats. In: Proceedings of the 10th Biennial International Conference on Engineering, Construction, and Operations in Challenging Environments and Second NASA/ARO/ASCE Workshop on Granular Materials in Lunar and Martian Exploration. Houston: ASCE, 2006, 1–8
18. Cooper K G, Good J E, Gilley S D. Layered metals fabrication technology development for support of lunar exploration at NASA/MSFC. AIP Conference Proceedings, 2007, 880: 728–735
19. Srivastava V, Lim S, Anand M. Microwave processing of lunar soil for supporting longer-term surface exploration on the Moon. Space Policy, 2016, 37: 92–96
20. Allan S M, Merritt B J, Griffin B F, Hintze P E, Shulman H S. High-temperature microwave dielectric properties and processing of JSC-1AC lunar simulant. Journal of Aerospace Engineering, 2013, 26(4): 874–881
21. Balla V K, Roberson L B, O'Connor G W, Trigwell S, Bose S, Bandyopadhyay A. First demonstration on direct laser fabrication of lunar regolith parts. Rapid Prototyping Journal, 2012, 18(6): 451–457
22. Goulas A, Engstrøm D S, Friel R J, Harris R A. Investigating the additive manufacture of extra-terrestrial materials. In: Proceedings of the 27th Annual International Solid Freeform Fabrication (SFF) Symposium—An Additive Manufacturing Conference. Austin: Laboratory for Freeform Fabrication and University of Texas at Austin, 2016, 2271–2281
23. Song L, Xu J, Tang H, Fan S Q, Liu J Z, Li X Y, Liu J Q. Research progress of simulated lunar soil molding. Acta Mineralogica Sinica, 2020, 40(1): 47–57 (in Chinese)
24. Toutanji H A, Evans S, Grugel R N. Performance of lunar sulfur concrete in lunar environments. Construction & Building Materials, 2012, 29: 444–448
25. Jakus A E, Koube K D, Geisendorfer N R, Shah R N. Robust and elastic lunar and Martian structures from 3D-printed regolith inks. Scientific Reports, 2017, 7: 44931
26. Toutanji H, Glenn-Loper B, Schrayshuen B. Strength and durability performance of waterless lunar concrete. In: Proceedings of the 43rd AIAA Aerospace Sciences Meeting and Exhibit. Reno: AIAA, 2005, AIAA 2005–1436
27. Liu M, Tang W Z, Duan W Y, Li S, Dou R, Wang G, Liu B S, Wang L. Digital light processing of lunar regolith structures with high mechanical properties. Ceramics International, 2019, 45(5): 5829–5836
28. Cesaretti G, Dini E, Kestelier X D, Colla V, Pambaguian L. Building components for an outpost on the lunar soil by means of a novel 3D printing technology. Acta Astronautica, 2014, 93: 430–450
29. Meurisse A, Makaya A, Willsch C, Sperl M. Solar 3D printing of lunar regolith. Acta Astronautica, 2018, 152: 800–810
30. Wang G, Zhao W, Liu Y F, Cheng T J. Review of space manufacturing technique and developments. SCIENTIA SINICA Physica, Mechanica & Astronomica, 2020, 50(4): 047006 (in Chinese)
31. Prater T, Werkheiser N, Ledbetter F, Timucin D, Wheeler K, Snyder M. 3D printing in zero G technology demonstration mission: complete experimental results and summary of related material modeling efforts. The International Journal of Advanced Manufacturing Technology, 2019, 101(1–4): 391–417
32. Reitz B, Lotz C, Gerdes N, Linke S, Olsen E, Pflieger K, Sohrt S, Ernst M, Taschner P, Neumann J, Stoll E, Overmeyer L. Additive manufacturing under lunar gravity and microgravity. Microgravity Science and Technology, 2021, 33(25): 1–12
33. Fateri M, Gebhardt A. Process parameters development of selective laser melting of lunar regolith for on-site manufacturing applications. International Journal of Applied Ceramic Technology, 2015, 12(1): 46–52
34. Yuan S Q, Chua C K, Zhou K, Bai J M, Wei J. Dynamic mechanical behaviors of laser sintered polyurethane incorporated with mwcnts. In: Proceedings of the 2nd International Conference on Progress in Additive Manufacturing (Pro-AM 2016). Singapore: Nanyang Technological University, 2016, 361–366
35. Li J, Yuan S Q, Zhu J H, Li S Y, Zhang W H. Numerical model and experimental validation for laser sinterable semi-crystalline polymer: shrinkage and warping. Polymers, 2020, 12(6): 1373
36. Yuan S Q, Li J, Yao X L, Zhu J H, Gu X J, Gao T, Xu Y J, Zhang W H. Intelligent optimization system for powder bed fusion of processable thermoplastics. Additive Manufacturing, 2020, 34: 101182
37. Yuan S Q, Li S Y, Zhu J H, Tang Y L. Additive manufacturing of polymeric composites from material processing to structural design. Composites Part B: Engineering, 2021, 219: 108903
38. Liu Y, Taylor L A. Characterization of lunar dust and a synopsis of available lunar simulants. Planetary and Space Science, 2011, 59(14): 1769–1783
39. Zheng Y C, Wang S J, Ouyang Z Y, Zou Y L, Liu J Z, Li C L, Li X Y, Feng J M. CAS-1 lunar soil simulant. Advances in Space Research, 2009, 43(3): 448–454
40. Tang H, Li X Y, Zhang S S, Wang S J, Liu J Z, Li S J, Li Y, Wu Y X. A lunar dust simulant: CLDS-i. Advances in Space Research, 2017, 59(4): 1156–1160
41. Sibille L, Carpenter P, Schlagheck R, French R A. Lunar Regolith Simulant Materials: Recommendations for Standardization, Production, and Usage. NASA Technical Reports NASA/TP-2006–214605, 2006
42. Indyk S J, Benaroya H. A structural assessment of unrefined sintered lunar regolith simulant. Acta Astronautica, 2017, 140: 517–536
43. Gualtieri T, Bandyopadhyay A. Compressive deformation of porous lunar regolith. Materials Letters, 2015, 143: 276–278
44. Li S Y, Yuan S Q, Zhu J H, Wang C, Li J, Zhang W H. Additive manufacturing-driven design optimization: building direction and structural topology. Additive Manufacturing, 2020, 36: 101406